Monthly Notices
of the
ROYAL ASTRONOMICAL SOCIETY
MNRAS **456,** L99–L103 (2016) doi:10.1093/mnrasl/slv179

Starbursting brightest cluster galaxy: a *Herschel* view of the massive cluster MACS J1931.8−2634

J. S. Santos,[1⋆] I. Balestra,[2⋆] P. Tozzi,[1⋆] B. Altieri,[3] I. Valtchanov,[3] A. Mercurio,[4] M. Nonino,[2] Heng Yu,[5,6,7] P. Rosati,[8] C. Grillo,[9] E. Medezinski[10,11] and A. Biviano[2]

[1]*INAF – Osservatorio Astrofisico di Arcetri, Largo Enrico Fermi 5, I-50125 Firenze, Italy*
[2]*INAF – Osservatorio Astronomico di Trieste, Via Tiepolo 11, I-34131 Trieste, Italy*
[3]*European Space Astronomy Centre (ESAC)/ESA, Villanueva de la Cañada, E-28691 Madrid, Spain*
[4]*INAF – Osservatorio Astronomico di Capodimonte, Salita Moiariello 16, I-80131 Napoli, Italy*
[5]*Department of Astronomy, Beijing Normal University, Beijing 100875, China*
[6]*Dipartimento di Fisica, Universitá di Torino, Via P. Giuria 1, I-10125 Torino, Italy*
[7]*Istituto Nazionale di Fisica Nucleare (INFN), Sezione di Torino, Via P. Giuria 1, I-10125 Torino, Italy*
[8]*Department of Physics and Earth Science, University of Ferrara, Via Saragat, 1, I-44122 Ferrara, Italy*
[9]*Dark Cosmology Centre, Niels Bohr Institute, University of Copenhagen, Juliane Maries Vej 30, DK-2100 Copenhagen, Denmark*
[10]*Center for Astrophysics and Planetary Science, Racah Institute of Physics, The Hebrew University, Jerusalem 91904, Israel*
[11]*Department of Physics and Astronomy, The Johns Hopkins University, 3400 North Charles Street, Baltimore, MD 21218, USA*

Accepted 2015 November 10. Received 2015 November 10; in original form 2015 August 17

ABSTRACT

We investigate the dust-obscured star formation (SF) properties of the massive, X-ray-selected galaxy cluster MACS J1931.8−2634 at $z = 0.352$. Using far-infrared (FIR) imaging in the range 100–500 μm obtained with the *Herschel* telescope, we extract 31 sources (2σ) within $r \sim 1$ Mpc from the brightest cluster galaxy (BCG). Among these sources, we identify six cluster members for which we perform an analysis of their spectral energy distributions (SEDs). We measure total infrared luminosity ($L_{\rm IR}$), star formation rate (SFR) and dust temperature. The BCG, with $L_{\rm IR} = 1.4 \times 10^{12}\,{\rm L}_{\odot}$ is an ultraluminous infrared galaxy and hosts a type-II active galactic nuclei (AGN). We decompose its FIR SED into AGN and starburst components and find equal contributions from AGN and starburst. We also recompute the SFR of the BCG finding SFR $= 150 \pm 15\ {\rm M}_{\odot}\ {\rm yr}^{-1}$. We search for an isobaric cooling flow in the cool core using *Chandra* X-ray data, and find no evidence for gas colder than 1.8 keV in the inner 30 kpc, for an upper limit to the instantaneous mass-deposition rate of $58\ {\rm M}_{\odot}\ {\rm yr}^{-1}$ at 95 per cent c.l. This value is 3× lower than the SFR in the BCG, suggesting that the on-going SF episode lasts longer than the intracluster medium cooling events.

Key words: galaxies: clusters: individual: MACS J1931.8−2634 – galaxies: star formation – infrared: galaxies – X-rays: galaxies: clusters.

1 INTRODUCTION

The cores of galaxy clusters are ubiquitously populated by old, passively evolving spheroids, with little evidence for ongoing or recent episodes of star formation (SF; e.g. Dressler 1980; Dressler et al. 1997; Von der Linden et al. 2010; Girardi et al. 2015). This suppression of SF is mainly caused by interactions among the densely packed galaxies (e.g. Moore et al. 1996; Gnedin 2003), and to a lesser extent by interactions between the hot, X-ray emitting intracluster medium (ICM) and the galaxies. The brightest cluster galaxy (BCG) that usually sits at the bottom of the potential well and is coincident with the peak of the cluster X-ray emission, is typically a very massive, bright, early-type galaxy, that only rarely is associated with significant SF activity (e.g. Samuele et al. 2011; Rawle et al. 2012; Fogarty et al. 2015).

Cool core (CC) clusters are systems whose ICM shows a minimum core temperature that is about one-third of the global ICM temperature and a low core entropy (<30 keV cm^2), that reflects significant radiative cooling taking place in the cluster innermost regions (e.g. Peterson & Fabian 2006; Hudson et al. 2010). Observations have shown that brightest cluster galaxy (BCGs) with ongoing SF activity are usually hosted by CC clusters (Hoffer et al. 2012). However, there is still a large variance in current results on the fraction of star-forming BCGs and the amount of their star formation rate (SFR). This is partly because different diagnostics are used [e.g. optical emission lines, UV continuum, far-infrared (FIR)] that

⋆ E-mail: jsantos@arcetri.astro.it (JSS); balestra@mpe.mpg.de (IB); ptozzi@arcetri.astro.it (PT)

may be affected by dust emission and active galactic nuclei (AGN) contamination, but also because samples are often not representative. In particular, Samuele et al. (2011) investigated the SF activity in a sample of 77 BCGs drawn from a flux-limited, X-ray-selected cluster sample and reported a lack of SF in that sample, based only on optical emission lines. In contrast, Rawle et al. (2012) detected SF in 15 out of 68 BCGs using a more robust diagnostic based on the FIR emission. The caveat in this fraction is that the sample of BCGs originate from a mix of cluster samples, mostly selected to include massive and relaxed clusters that are thus biased towards CCs, therefore are more likely associated with star-forming BCGs.

It is well known that AGN play a crucial role in the regulation of the SF in BCGs (e.g. Hlavacek-Larrondo et al. 2013; Russell et al. 2013). Ample evidence for AGN feedback has been collected in the last decade, where radio jets have been shown to inflate bubbles in the ICM and hence offset cooling, nonetheless the link between AGN and SF is not yet properly established (e.g. McNamara & Nulsen 2007, for a review). The recent study of the Phoenix cluster at $z = 0.596$ (McDonald et al. 2012), the strongest CC cluster known to date, showed a BCG with a very high SFR and an equally significant AGN activity.

The X-ray-selected cluster MACS J1931.8−2634 (MACS1931 hereafter; Ebeling et al. 2001) at $z = 0.352$ is part of the Cluster Lensing And Supernova survey with Hubble (CLASH; Postman et al. 2012) sample of 25 massive clusters used to study the distribution of dark matter in clusters. As all of the CLASH clusters, MACS1931 is massive with $M_{200} = 9.9 \pm 0.7 \times 10^{14}$ $M_\odot$ (Merten et al. 2015) with a relaxed X-ray morphology, and harbours a CC (Ehlert et al. 2011). The cluster is dominated by a very large, luminous central galaxy that, contrary to what is common in most massive clusters, is undergoing a phase of copious SF. Measured star formation rates (SFRs) range from 80 $M_\odot$ yr^{-1} (rest-frame UV imaging; Donahue et al. 2015) to 170 $M_\odot$ yr^{-1} (broad-band optical imaging; Ehlert et al. 2011). However, these SFRs may be contaminated by AGN activity and underestimated due to dust obscuration.

The work presented in this Letter aims to overcome these two biases. We present the analysis of *Herschel* (Pilbratt et al. 2010) 100–500 μm observations of MACS1931 that cover the peak of the SED of starbursts. The FIR is the best diagnostic for SF as it provides a direct measure of the reprocessed UV light from the on-going SF, allowing us to measure the total FIR luminosity, SFRs and dust temperatures of the cluster members. We also focus on the BCG and its environment using *Chandra* X-ray data. The work presented here is part of a larger *Herschel* study including all CLASH clusters. The cosmological parameters used throughout the Letter are: $H_0 = 70$ h km s^{-1} Mpc^{-1}, $\Omega_\Lambda = 0.7$ and $\Omega_m = 0.3$.

2 DATA

Although this work is focused on data from the *Herschel* space telescope, we use ample ancillary data both proprietary and archival: mid-infrared data from Wide-Field Infrared Survey Explorer (*WISE*); X-ray data from *Chandra*; optical data from Subaru (BVR$_c$I$_c$z), the *Hubble Space Telescope* (*HST*), and extensive VLT/VIMOS spectroscopy.

2.1 *Herschel* observations and data reduction

The *Herschel* observations of MACS1931 were carried out in 2011, 2012 and 2013 as Open Time 1 and 2 programmes (PI Egami, obsid = 1342215993, 1342241619, 1342241681, 1342254639) aimed at studying the SF properties of lensing clusters. The Photoconductor Array Camera and Spectrometer (PACS) (Poglitsch et al. 2010) observations at 100 and 160 μm were performed in scan map mode. The maps were produced using UNIMAP (Piazzo et al. 2015): a generalized least square map-maker, that allows us to reach ultimate sensitivity with no flux loss, and without iterative masking of the sources. The 1σ noise of the maps is 1.6 mJy in the 100 μm band and 3.5 mJy in the 160 μm image. Spectral and Photometric Imaging Receiver (SPIRE) (Griffin et al. 2010) maps with an ∼5 arcmin radius were obtained in small map mode. The SPIRE maps at 250, 350 and 500 μm with nominal pixel sizes of 6, 10 and 14 arcsec, respectively, are dominated by confusion noise with an rms in the centre of 6.2, 6.5 and 7.3 mJy.

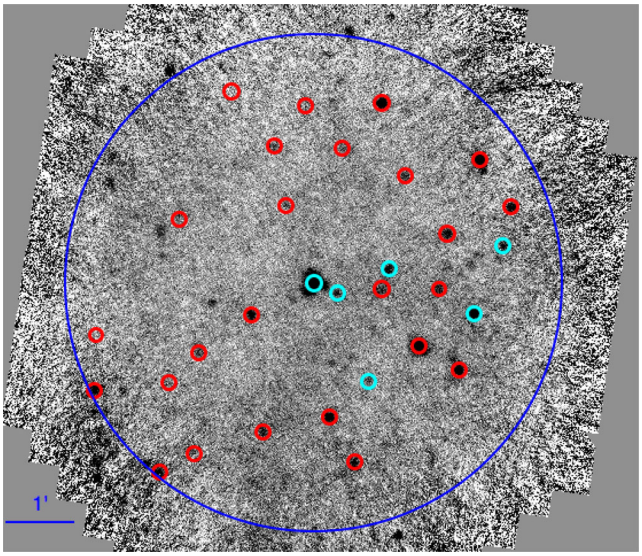

Figure 1. PACS 100 μm image of the cluster field centred on the BCG. The blue circle with $r \sim 1$ Mpc (∼1/2 of r_{200}) indicates the region of source extraction. The small (6 arcsec radius) circles represent the 31 individual FIR sources in our catalogue (cluster members are highlighted in cyan). North is up and east to the left.

2.2 Far-infrared sources in MACS1931

Our FIR observations of MACS1931 covers a region with 3.6 arcmin radius centred on the X-ray cluster centre, where the sensitivity of the PACS maps is robust (see Fig. 1). This radius corresponds to 1.1 Mpc in physical units which is about 1/2 of the cluster virial radius measured from lensing ($r_{200} = 1.82 \pm 0.04$ Mpc; Merten et al. 2015).

Here we outline our procedure to obtain the catalogue of FIR sources in the field of MACS1931. Our catalogue is based on blind source detections in the 100 and 160 μm maps separately, using SExtractor (Bertin & Arnouts 1996). As standard for PACS data, the photometry is made with fixed apertures with radii of 6 and 9 arcsec at 100 and 160 μm, respectively, corrected with the encircled energy factors given by Balog et al. (2014). This procedure was validated with manual aperture photometry. Given the difficulty to obtain reliable errors with standard source detection algorithms because of the correlated noise present in PACS data, we compute the photometric errors as the 1σ detection limits in each band, in addition to 7 per cent (calibration accuracy of the flux scale) of the source flux. The SPIRE source detection was performed using a simultaneous fit to all sources in the prior list based on the PACS detections. We run the XID method (Roseboom et al. 2012)

Table 1. Properties of the FIR cluster members, with spectroscopic redshift and photometric redshift concordant with the cluster.

ID	RA	Dec.	z	$r_{\rm proj}$ (kpc)	$F_{100\,\mu m}$ (mJy)	$F_{160\,\mu m}$ (mJy)	LIR ($\times 10^{11}$ L$_\odot$)	SFR (M$_\odot$ yr^{-1})	$T_{\rm dust}$ (K)
62	292.905501	−26.5669131	0.3644	923	6.5 ± 1.7	9.6 ± 3.6	0.43 ± 0.04	6.4 ± 0.6	29 ± 5
69 (BCG)	292.956707	−26.5758907	0.352	–	212.5 ± 15.0	231.3 ± 16.5	14 ± 2	210 ± 23	33 ± 2
75*	292.950604	−26.5782649	0.3652	117	3.2 ± 1.6	10.7 ± 3.6	0.47 ± 0.07	7.0 ± 1.5	14 ± 1
89	292.941855	−26.5994976	0.3494	498	4.0 ± 1.6	10.1 ± 3.6	0.34 ± 0.04	5.0 ± 0.5	24 ± 4
68	292.936482	−26.5724383	0.36 ± 0.07	366	8.9 ± 1.7	12.4 ± 3.6	0.54 ± 0.06	8.0 ± 1.0	30 ± 4
80	292.913344	−26.5832069	0.34 ± 0.07	785	21.5 ± 2.2	32.2 ± 4.2	1.3 ± 0.1	19.5 ± 1.7	29 ± 2

Notes. *SPIRE fluxes of ID 75 may be contaminated by the BCG that is located at ∼20 arcsec distance.

using the same prior catalogue on the three SPIRE bands, using the corresponding SPIRE point response function for each band. If the fitted SPIRE flux density at the position of an input PACS source is below the 3σ sensitivity in each band we assigned the 3σ values as upper limits. These correspond to $3\times$ the confusion noise and are equal to 17.4, 18.9 and 20.4 mJy at 250, 350 and 500 μm, respectively.

We obtain 31 detections at $>2\sigma$ in at least one of the PACS bands, within $r = 3.6$ arcmin centred on the BCG. To identify the origin of these sources, we match the FIR catalogue with our spectroscopic and photometric redshift catalogues. The spectroscopic catalogue consists of 2800 redshifts obtained with VIMOS (CLASH-VLT Large Programme 186.A-0798, PI Rosati; Rosati et al. 2014), whereas the photo-z catalogues are based on photometry from the *HST* and Subaru.[1] We find that, of the 31 sources in the cluster field, 4 are confirmed members, 2 are candidate members (photo-z) and 18 are interlopers. Since the completeness of our spectroscopic sample of cluster members is close to 90 per cent it is unlikely that the remaining seven *Herschel* sources are at the cluster redshift.

3 FAR-INFRARED PROPERTIES OF THE CLUSTER GALAXIES

We fit the galaxies FIR SEDs using LEPHARE (Arnouts et al. 1999) with Chary & Elbaz (2001) templates, to measure the galaxy-integrated infrared luminosity $L_{\rm IR}$ in the range 8–1000 μm. The SFRs are derived using the updated scaling relation, $\mathrm{SFR_{IR}} = 1.48 \times 10^{-10} L_{\rm IR}/\mathrm{L_\odot}$, (Kennicutt & Evans 2012; Murphy et al. 2011; Hao et al. 2011) that uses a Kroupa initial mass function (Kroupa & Weidner 2003).[2] The SFR of our sample, measured with pure starburst templates, spans the range 5–210 M$_\odot$ yr^{-1}. If we exclude the highest star-forming galaxy – the BCG – we find an average SFR of 9.2 M$_\odot$ yr^{-1}. The total SFR of the six cluster galaxies amounts to 256 M$_\odot$ yr^{-1}. This value is in good agreement with the recent result on the SFR of massive clusters using *Herschel* data by Popesso et al. (2015). In the next section, we perform a more detailed study of the BCG and refine its SFR measure, after accounting for the impact of the AGN. With the exception of the BCG that is an ultraluminous infrared galaxy (ULIRG, $\gtrsim 10^{12}$ L$_\odot$), the FIR-detected cluster galaxies are LIRGs or normal star-forming galaxies.

The temperature of the dust, $T_{\rm dust}$, present in the galaxies is computed with a modified blackbody model with an emissivity index β fixed to 1.5. Apart from galaxy ID 75, that shows some contamination with the BCG fluxes in the SPIRE bands, we find $T_{\rm dust}$ in the range 24–33 K, which is within the range of dust temperatures for $z \leq 0.3$ LIRGs and ULIRGs (Magdis et al. 2014). The FIR properties of the cluster members are summarized in Table 1.

4 CONNECTION BETWEEN THE BCG, THE AGN AND THE ICM

In this section, we analyse in detail the BCG sitting at the core of the cluster. It is uncommon to have a cluster with a massive BCG with an SFR level of 210 M$_\odot$ yr^{-1} (Hoffer et al. 2012; Rawle et al. 2012). However, our initial SFR result may be biased by the presence of a strong obscured AGN, which needs to be carefully modelled. We also explore the interconnections between the SF of the BCG and the mass deposition rate in the cluster core. The UV and optical properties of this galaxy have been studied in Donahue et al. (2015) and Ehlert et al. (2011), that computed the galaxy SFR using different diagnostics. We convert their values to the ones obtained with the updated calibration used here, as described in Kennicutt & Evans (2012). While Donahue et al. (2015) found an SFR = 69 M$_\odot$ yr^{-1} using UV photometry, Ehlert et al. (2011), in a crude approximation, derived a value twice larger, 146 M$_\odot$ yr^{-1}, based on optical broad-band imaging. These calculations do not account for dust extinction nor for contamination from AGN activity.

4.1 SED decomposition: AGN and star formation

The BCG of MACS1931 hosts an X-ray bright AGN, embedded in the ICM emission, which we model and subtract from the AGN signal. We detect about 1030 counts in the 0.5–7 keV band. Our spectral analysis with an intrinsic slope fixed to $\Gamma = 1.8$, provides an intrinsic absorption of $N_H = 1.94^{+0.21}_{-0.19} \times 10^{22}$ cm^{-2}, which is very close to the canonical value 10^{22} cm^{-2} above which an AGN is classified as absorbed. The unabsorbed rest-frame luminosities are $L_{0.5-2\,\mathrm{keV}} = 3.6 \times 10^{43}$ erg s^{-1} and $L_{2-10\,\mathrm{keV}} = 6.9 \times 10^{43}$ erg s^{-1}.

We first investigate the contribution of the AGN component to the FIR emission using DECOMPIR (Mullaney et al. 2011), an SED model-fitting software that decomposes the FIR SED in AGN and starburst components. In short, the AGN component is an empirical model based on observations of moderate-luminosity local AGNs, whereas the five starburst models represent a typical range of SED types, with an extrapolation beyond 100 μm using a grey body with $\beta = 1.5$. The best-fitting model obtained with DECOMPIR considering the *Herschel* data points (Fig. 2) yields $L_{\rm IR} = 2.2 \times 10^{12}$ L⊙, with AGN and starburst contributions of 53 per cent and 47 per cent, respectively. This allows us to recompute the SFR removing the AGN contamination. We thus obtain SFR (BCG) = 150 ± 15 M$_\odot$ yr^{-1}, a value similar to that reported in Ehlert et al. (2011) but much more robust.

[1] CLASH catalogues: https://archive.stsci.edu/prepds/clash/

[2] These SFRs are lower than the ones obtained with the widely used Kennicutt 1998 calibration (SFR = 0.86 × SFR$_{K98}$)

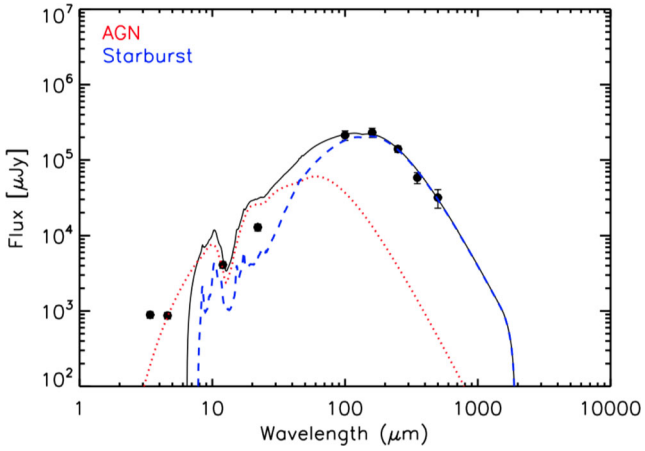

Figure 2. Infrared SED of the BCG. Black points show the observed data from *WISE* and *Herschel* and the black solid line represents the best-fitting SED model. AGN and starburst components from the combined SED are shown in red and blue, respectively.

4.2 Mass deposition rate and SFR

MACS1931 harbours one of the most X-ray luminous CCs known. The properties of the core of MACJ1931 have been investigated in detail in Ehlert et al. (2011), where an equivalent mass deposition rate of $\sim$700$M_\odot$ yr^{-1} in the inner 70 kpc has been estimated in the assumption of isobaric cooling. Despite the high cooling rate, this cluster is missing the central metallicity peak which is otherwise measured in the majority of CC clusters (De Grandi et al. 2004). This suggests bulk transport of cool gas out to large distances from the centre due to the powerful AGN outburst (Ehlert et al. 2011). In particular, a bright, dense region, north of the BCG, shows low-temperature and high-density metal-rich gas and is consistent with being a remnant of the CC after it was disrupted by the AGN (see also Kirkpatrick et al. 2011).

We constrain the ICM mass cooling rate, $\dot{M}$, in the inner 30 kpc around the BCG under the same assumption of isobaric cooling. The main difference relative to the previous analysis by Ehlert et al. (2011) is that we focus on a limited temperature range, 0.15–3.0 keV, and in particular below 1.8 keV. In fact, the signature of an isobaric cooling flow is given by a specific relation between the emission measure and the gas temperature, as described in the model mkcflow (Mushotzky & Szymkowiak 1988). Therefore, we measure the cooling rate of the gas independently in five temperature bins, using a set of mkcflow models within XSPEC (Arnaud 1996) in the following temperature intervals: 0.15–0.25, 0.25–0.45, 0.45–0.9, 0.9–1.8 and 1.8–3.0 keV. We also consider a single temperature MEKAL (Mewe, Gronenschild & van den Oord 1985, Mewe, Lemen & van den Oord 1986, Kaastra 1992, Liedahl, Osterheld & Goldstein 1995) component to account for the gas hotter than 3 keV. We detect about 13 700 net counts (0.5–7.0 keV band) in the inner 30 kpc. Since it is not possible to measure the metal abundance of the cold gas, given its low emission measure, we conservatively assume that its metallicity is equal to that of the MEKAL component which dominates the emission, which is $Z = 0.35 \pm 0.05\,Z_\odot$. We find that the mass deposition rate for gas below 3 keV has a 95 per cent single-sided upper limit of $\dot{M} < 135\,M_\odot$ yr^1 (see dashed horizontal line in Fig. 3, left-hand panel), while the temperature of the MEKAL component is $kT = 6.43^{+0.50}_{-0.45}$ keV. When we try to constrain $\dot{M}$ in temperature intervals, we find that we are able to measure a substantial mass deposition rate only in the temperature range 1.8–3.0 keV. Below 1.8 keV, the upper limit on the mass deposition rate is only $\dot{M} < 58\,M_\odot$ yr^1 at a 95 per cent c.l. The upper limits measured in different temperature bins are shown in Fig. 3, left-hand panel. We find that $\dot{M}$ is significantly lower – at least by a factor of 3 – than the measured SFR.

This result is in broad agreement with the correlation between the SFR observed in the BCG and the properties of the hosting CC (Rafferty et al. 2006; Rawle et al. 2012), but in disagreement with previous measurements of a mass deposition rate typically higher than the SFR in the BCG (O'Dea et al. 2008; McDonald et al. 2011; Mittal et al. 2015). Clearly, the ratio of the mass deposition rate and the SFR is sensitive to the time-scales for ICM cooling and SF and it is not expected to vary much among clusters. To check whether we can reconcile the results for MACSJ1931 with previous results, we also explore the presence of colder clouds (with temperature $<10^7$ K) in the ICM beyond 30 kpc, where a significant fraction of colder gas can cool and fall into the innermost regions. This is suggested by a recent work by Voit et al. (2015) which showed that colder clouds can precipitate out of the hot gas via thermal instability on a large region centred in the core, feeding black hole accretion and/or SF in the BCG. Even in this case we find an upper limit (95 per cent c.l.) of 45 and 52 $M_\odot$ yr^{-1} in annuli of 30–50 and 50–70 kpc, respectively. Therefore, we do not find evidence of a large amount of colder gas within 30 kpc nor

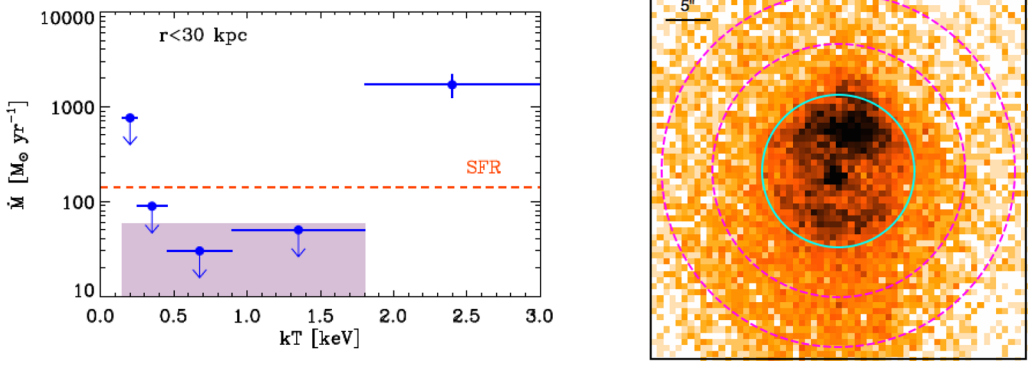

Figure 3. Left: $\dot{M}/M_\odot$ (blue circles) measured in different temperature bins in the inner 30 kpc of MACJ1931. Errors bars correspond to 1σ while arrows indicate single-sided 95 per cent upper limits. The shaded area is the single-sided 95 per cent upper limit on the global mass cooling rate obtained with a single mkcflow model in the temperature range 0.15–1.8 keV. The horizontal line marks the star formation rate of the BCG. Right: soft X-ray band (0.5 arcmin × 0.5 arcmin) centred on the BCG. The regions in which we computed $\dot{M}$ are shown in cyan (inner 30 kpc) and in magenta (annulus with 50–70 kpc radius). North is up and east to the left.

falling from beyond 30 kpc on to the centre. The low upper limits on the mass deposition rate found in the case of MACSJ1931, may require a scenario where the time-scale for SFR in the BCG is longer than the cooling events occurring intermittently in the cluster core. To investigate this possibility, we are currently exploring the relation between $\dot{M}$ and SFR in a small sample of nearby clusters whose BCG shows significant SF (Molendi et al., in preparation).

5 CONCLUSIONS

In this Letter, we present a study of the dust obscured SF properties in the galaxy cluster MACS1931 at $z = 0.352$, and a detailed investigation on the origin of the BCG SFR. We detect FIR emission in six cluster members and we derive SFRs based on broad-band FIR SEDs in the range 5–150 $M_\odot$ yr^{-1}, and dust temperatures in the range 24–33 K. The strongest *Herschel* source in the cluster field is, notably, the BCG, one of the few ULIRGs detected in the nearby Universe. Our analysis shows the importance of adequately assessing the contamination from AGN, but even accounting for ∼50 per cent of L_{IR} due to the AGN, we estimate an SFR = 150 $M_\odot$ yr^{-1} for the BCG, a surprising value for a galaxy expected to be 'red and dead'. At similar redshift only Abell 1835 has a comparable SFR. At the same time, cold gas (kT < 1.8 keV) is not detected in the ICM gas, and the mass deposition rate has a robust upper limit of 58 $M_\odot$ yr^{-1}, suggesting that in this case SF lasts longer than the ICM cooling events.

ACKNOWLEDGEMENTS

We thank G. Risaliti, G. Giovannini, E. Liuzzo and M. Massardi for useful discussions on the AGN properties. We also thank the anonymous referee for useful comments. JSS and IB acknowledge funding from the European Union Seventh Framework Programme (FP7/2007-2013) under grant agreement nr 267251 'Astronomy Fellowships in Italy' (AstroFIt). We acknowledge financial support from PRIN INAF 2012 A unique data set to address the most compelling open questions about X-ray galaxy clusters and PRIN-INAF 2014: Glittering Kaleidoscopes in the sky, the multifaceted nature and role of galaxy clusters. Results are partly based on ESO LP186.A-0798. *Herschel* is an ESA space observatory with science instruments provided by European-led PI consortia and with important participation from NASA.

REFERENCES

Arnaud K. A., 1996, ASP Conf. Ser. Vol. 101, Astronomical Data Analysis Software and Systems V. Astron. Soc. Pac., San Francisco, p. 17
Arnouts S., Cristiani S., Moscardini L., Matarrese S., Lucchin F., Fontana A., Giallongo E., 1999, MNRAS, 310, 540
Balog Z. et al., 2014, Exp. Astron., 37, 129
Bertin E., Arnouts S., 1996, A&AS, 117, 393
Chary R., Elbaz D., 2001, ApJ, 556, 562
De Grandi S., Ettori S., Longhetti M., Molendi S., 2004, A&A, 419, 7
Donahue M. et al., 2015, ApJ, 805, 177
Dressler A., 1980, ApJ, 236, 351
Dressler A. et al., 1997, ApJ, 490, 577
Ebeling H., Jones L. R., Fairley B. W., Perlman E., Scharf C., Horner D., 2001, ApJ, 548, L23
Ehlert S. et al., 2011, MNRAS, 411, 1641
Fogarty K., Postman M., Connor T., Donahue M., Moustakas J., 2015, ApJ, 813, 117
Girardi M. et al., 2015, A&A, 579, A4
Gnedin O. Y., 2003, ApJ, 589, 752
Griffin M. J. et al., 2010, A&A, 518, L3
Hao C.-N., Kennicutt R. C., Johnson B. D., Calzetti D., Dale D. A., Moustakas J., 2011, ApJ, 741, 124
Hlavacek-Larrondo J., Fabian A. C., Edge A. C., Ebeling H., Allen S. W., Sanders J. S., Taylor G. B., 2013, MNRAS, 431, 1638
Hoffer A. S., Donahue M., Hicks A., Barthelemy R. S., 2012, ApJS, 199, 23
Hudson D. S., Mittal R., Reiprich T. H., Nulsen P. E. J., Andernach H., Sarazin C. L., 2010, A&A, 513, A37
Kaastra J. S., 1992, An X-Ray Spectral Code for Optically Thin Plasmas (Internal SRON-Leiden Report, updated version 2.0)
Kennicutt R. C., Jr, 1998, ARA&A, 36, 189
Kennicutt R. C., Evans N. J., 2012, ARA&A, 50, 531
Kirkpatrick C. C., McNamara B. R., Cavagnolo K. W., 2011, ApJ, 731, L23
Kroupa P., Weidner C., 2003, ApJ, 598, 1076
Liedahl D. A., Osterheld A. L., Goldstein W. H., 1995, ApJ, 438, L115
McDonald M., Veilleux S., Rupke D. S. N., Mushotzky R., Reynolds C., 2011, ApJ, 734, 95
McDonald M. et al., 2012, Nature, 488, 349
McNamara B. R., Nulsen P. E. J., 2007, ARA&A, 45, 117
Magdis G. et al., 2014, ApJ, 796l, 63
Merten J. et al., 2015, ApJ, 806, 4
Mewe R., Gronenschild E. H. B. M., van den Oord G. H. J., 1985, A&AS, 62, 197
Mewe R., Lemen J. R., van den Oord G. H. J., 1986, A&AS, 65, 511
Mittal R., Whelan J. T., Combes F., 2015, MNRAS, 450, 2564
Moore B., Katz N., Lake G., Dressler A., Oemler A., 1996, Nature, 379, 613
Mullaney J. R., Alexander D. M., Goulding A. D., Hickox R. C., 2011, MNRAS, 414, 1082
Murphy E. J. et al., 2011, ApJ, 737, 67
Mushotzky R. F., Szymkowiak A. E., 1988, Proc. NATO Adv. Res. Workshop, Vol. 229, Cooling Flows in Clusters and Galaxies. Kluwer, Dordrecht, p. 53
O'Dea C. P. et al., 2008, ApJ, 681, 1035
Peterson J. R., Fabian A. C., 2006, Phys. Rep., 427, 139
Piazzo L., Calzoletti L., Faustini F., Pestalozzi M., Pezzuto S., Elia D., di Giorgio A., Molinari S., 2015, MNRAS, 447, 1471
Pilbratt G. L. et al., 2010, A&A, 518, L1
Poglitsch A. et al., 2010, A&A, 518, L2
Popesso P. et al., 2015, A&A, 579, A132
Postman M. et al., 2012, ApJS, 199, 25
Rafferty D. A., McNamara B. R., Nulsen P. E. J., Wise M. W., 2006, ApJ, 652, 216
Rawle T. D. et al., 2012, ApJ, 747, 29
Rosati P. et al., 2014, The Messenger, 158, 48
Roseboom I. et al., 2012, MNRAS, 419, 2758
Russell H. R., McNamara B. R., Edge A. C., Hogan M. T., Main R. A., Vantyghem A. N., 2013, MNRAS, 432, 530
Samuele R., McNamara B. R., Vikhlinin A., Mullis C. R., 2011, ApJ, 731, 31
Voit G. M., Donahue M., Bryan G. L., McDonald M., 2015, Nature, 519, 203
von der Linden A., Wild V., Kauffmann G., White S. D. M., Weinmann S., 2010, MNRAS, 404, 1231

This paper has been typeset from a TEX/LATEX file prepared by the author.